Inorganic Chemistry

Article

pubs.acs.org/IC

Synthesis, Crystal Structure, Transport, and Magnetic Properties of Novel Ternary Copper Phosphides, $A_2Cu_6P_5$ (A = Sr, Eu) and $EuCu_4P_3$

Dmitri O. Charkin,[†,*] Arthur V. Urmanov,[†] Sergey M. Kazakov,[†] Dmitri Batuk,[‡] Artem M. Abakumov,[†,‡] Stephan Knöner,[§] Elena Gati,[§] Bernd Wolf,[§] Michael Lang,[§] Andrey V. Shevelkov,[†] Gustaaf Van Tendeloo,[‡] and Evgeni V. Antipov[†]

[†]Department of Chemistry, M.V. Lomonosov Moscow State University, 119991 Moscow, Russia

[‡]Electron Microscopy for Materials Research (EMAT), University of Antwerp, Groenenborgerlaan 171, B-2020 Antwerp, Belgium

[§]Physikalisches Institut, Universität Frankfurt, Max-von-Laue Strasse 1, 60438 Frankfurt, Germany

Supporting Information

ABSTRACT: Three new ternary copper phosphides, $Sr_2Cu_6P_5$, $Eu_2Cu_6P_5$, and $EuCu_4P_3$, have been synthesized from the elements in evacuated silica capsules. $Eu_2Cu_6P_5$ and $Sr_2Cu_6P_5$ adopt the $Ca_2Cu_6P_5$-type structure, while $EuCu_4P_3$ is isostructural to $BaMg_4Si_3$ and still remains the only representative of this structure type among the ternary Cu pnictides. All three materials show metallic conductivity in the temperature range 2 K ≤ T ≤ 290 K, with no indication for superconductivity. For $Eu_2Cu_6P_5$ and $EuCu_4P_3$, long-range magnetic order was observed, governed by 4*f* local moments on the Eu atoms with predominant ferromagnetic interactions. While $Eu_2Cu_6P_5$ shows a single ferromagnetic transition at T_C = 34 K, the magnetic behavior of $EuCu_4P_3$ is more complex, giving rise to three consecutive magnetic phase transitions at 70, 43, and 18 K.

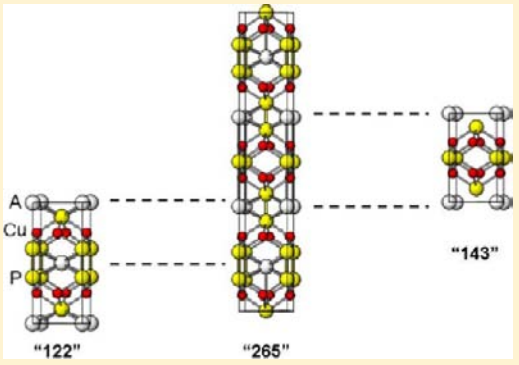

INTRODUCTION

The recent discovery of superconductivity with T_c up to 55 K in layered iron chalcogenides and pnictides[1] initiated intensive research on both novel FeAs-based superconductors and other chemical compositions which could, due to the slabs of condensed TX_4 (T − transition metal, X − chalcogen or pnicogen) tetrahedra, give rise to new families of superconductors. For the 3*d*-metal-bearing compounds, low-temperature superconducting properties have been found for nickel (see the review[2] and references therein) and recently for copper in a yet unique $LiCu_2P_2$[3a] compound of a $ThCr_2Si_2$-type ("122" type). This is in fair agreement with the theoretical considerations[4] that suggest that superconductivity can be observed in the vicinity of a magnetic instability, which is the case for the Fe, Ni, and Cu pnictides. Layered multinary Cu pnictides exhibit a relatively rich structural chemistry approaching that of the related Fe compounds.[5−11] The Cu oxypnictides are well studied and do not exhibit superconductivity; much less is known about the ternaries. Several structure types are represented by one or two compounds; this also complicates their crystal chemistry analysis because the links between the structure types are hard to establish.

In the present paper, we report on new layered phosphides of copper, alkaline earth metals, and europium. The majority of these compounds belong to the $ThCr_2Si_2$ ($ACu_{2-x}Pn_2$[8−10]) structure except $Ca_2Cu_6P_5$ ("265"),[10] which is an intergrowth of the "122" and "143" types (Figure 1). Up to now, the latter "143" structure was observed for the $BaMg_4Tt_3$ tetrelides (Tt = Si, Ge)[12] but not for Cu pnictides. Therefore, we performed a search for new "143" and "265" compounds in the A−Cu−Pn systems (A = Ca, Sr, Ba, Eu; Pn = P, As).

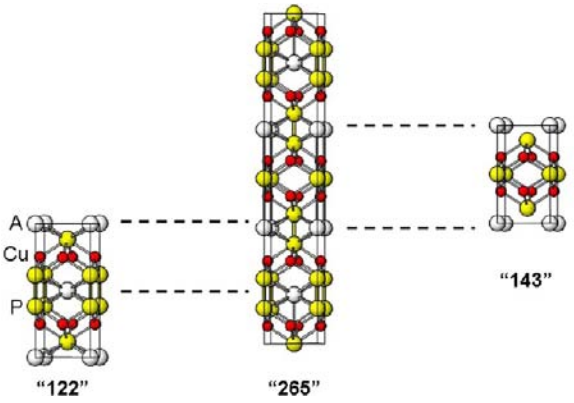

Figure 1. Structural relations in the Eu−Cu−P system (Eu, gray; Cu, red; P, yellow).

EXPERIMENTAL SECTION

Synthesis. The elements (purity >99%) were used as starting materials. All operations were carried out in an argon-filled M'Braun glovebox (O_2 and H_2O content below 5 ppm). Ca, Sr, Ba, and Eu

Received: May 18, 2012
Published: July 31, 2012

   dx.doi.org/10.1021/ic301033h | *Inorg. Chem.* 2012, 51, 8948−8955

chunks were chopped and mixed with copper powder and phosphorus (violet) in the desired proportions. The mixtures were cold-pressed at ca. 8 t/cm^2 for 0.5−1 min and annealed in carbon-lined evacuated (5−10 Pa) silica capsules. Because of the low melting points and the volatile nature of possible intermediate products, the first annealing procedure consisted of three 12 h (at 200, 400, and 600 °C) and one 48 h (800 °C) plateaus; the heating ramp between the plateaus was 20°/h. After that, two regrindings and reannealings were performed at 900 °C for 20 h with a heating rate of 100 °C/h. The resulting compounds are black powders stable in closed vials for months.

X-ray Powder Diffraction. Powder X-ray diffraction data were collected on a Bruker D8 Advance diffractometer (Cu $K\alpha_1$ radiation, Ge-(111) monochromator, reflection geometry, LynxEye silicon strip detector) in the angular range of 2θ = 5°−100° with a step size of 0.015° and collection time of 2 s per step.

Rietveld refinements were performed with the TOPAS package[13] using the fundamental parameter approach for the peak shape description. The structural models proposed by Pilchowski et al.[10] for $Ca_2Cu_6P_5$ and by Zürcher et al.[12] for $BaMg_4Si_3$ were used as the starting atomic parameter values for $Eu_2Cu_6P_5$ and $EuCu_4P_3$, respectively. The preferred orientation was corrected using a spherical harmonics approach implemented in TOPAS. A small level of impurities (CuP_2 for both compounds and $EuCu_4P_3$ in the case of $Eu_2Cu_6P_5$) was found in the XRD data, and these phases were included into the refinements. The structural data and selected bond distances are presented in Tables 1−4. Final Rietveld refinement plots are given in Figure 2. Full program outputs are presented in the Supporting Information.

Table 1. Structural Data for $Sr_2Cu_6P_5$, $Eu_2Cu_6P_5$ and $EuCu_4P_3$

	$Sr_2Cu_6P_5$	$Eu_2Cu_6P_5$	$EuCu_4P_3$
Crystal system	tetragonal		
Space group	*I*4/*mmm* (# 139)		*P*4/*mmm* (# 129)
Cell parameters			
a, Å	4.1183(1)	4.07447(4)	4.05761(5)
c, Å	24.637(1)	24.6121(3)	7.4392(1)
V, Å^3	418.26(1)	408.59(1)	122.48(3)
Z	2		1
Calculated density, g/cm^3	5.649(2)	6.828(2)	6.766(3)
2ϑ range	5−100		
R values:			
R_B	0.020	0.019	0.007
R_p	0.038	0.027	0.035
R_{wp}	0.058	0.033	0.041
GOF	2.85	1.21	1.16

Transmission Electron Microscopy. Specimens for transmission electron microscopy (TEM) were prepared by crushing powder samples in methanol and depositing drops of the suspension on holey carbon grids. Selected area electron diffraction (SAED) patterns and high-angle annular dark-field scanning transmission electron microscopy (HAADF-STEM) images were recorded on a FEI Tecnai G2 microscope operated at 200 kV. The HAADF-STEM images simulation was conducted with QSTEM software, employing the multislice algorithm.[14]

Table 3. Refined Atomic Parameters for $EuCu_4P_3$

Atom	*x*	*y*	*z*	Occ	B_{eq}, Å^2
Eu	0	0	0	1	0.3(2)
Cu	1/2	0	0.3268(3)	1.00(2)	0.9(2)
P1	0	0	1/2	1	0.6(2)
P2	1/2	1/2	0.1515(8)	1	0.4(2)

Table 4. Selected Bond Distances for Eu-122,[6] Eu-265, and Eu-143

d, Å	$EuCu_{2-x}P_2$	$Eu_2Cu_6P_5$	$EuCu_4P_3$
Eu−P (toward Cu_2P_2)	3.122 × 8	3.132(4) × 4	
(toward Cu_4P_3)		3.067(3) × 4	3.083(2) × 8
Cu−P (within Cu_2P_2)	2.409 × 4	2.407(5) × 4	
(toward outer P in Cu_4P_3)		2.438(6) × 2	2.412(3) × 2
(toward inner P in Cu_4P_3)		2.403(2) × 2	2.404(1) × 2
P−P	2.283 × 1	2.270(10) × 1	2.254(8) × 1

Magnetic Measurements. The temperature dependence of the magnetic susceptibiliy $\chi(T)$ was determined in the temperature range 2 K ≤ *T* ≤ 290 K by using a Quantum-Design SQUID magnetometer (MPMS-XL5), employing a small applied field of 5 mT. The magnetic signal of the empty sample holder and the diamagnetic core contribution according to tabulated values[15] were subtracted from the experimental data. Isothermal magnetization measurements were performed in fields up to 5 T. The masses of the pressed powder samples were 46.4 mg for $EuCu_4P_3$ and 80.3 mg for $Eu_2Cu_6P_5$. The specimens were block-like with somewhat irregular shape. According to the formal oxidation states of 2+ for Sr and 1+ for Cu in $Sr_2Cu_6P_5$, a purely diamagnetic behavior for this compound is expected. For this reason, we refrained from performing a detailed magnetic characterization of this compound.

Resistivity Measurements. The temperature-dependent electrical resistivity was measured in the range 2 K ≤ *T* ≤ 290 K by employing a standard 4-terminal *dc* technique. Rod-shaped specimens with a typical size of 3 mm × 3 mm × 1 mm were cut from the sintered samples. For the electrical contacts, Au wires (diameter 25 μm) were glued to the sample using silver paste. Temperature sweeps were performed with a rate of 0.3 K/min to ensure thermal equilibrium. Current−voltage (*I*−*V*) characteristics were taken prior to the measurements to ensure that for the applied current, the samples are in the ohmic regime, i.e., $V \propto I$.

RESULTS

New Compounds and Structures. The powder XRD data indicate the formation of two new "265" type compounds, $Sr_2Cu_6P_5$ and $Eu_2Cu_6P_5$, as well as one "143" type phosphide, $EuCu_4P_3$. In the case of other starting compositions (all Ba- and As-containing samples, as well as "143" for Ca and Sr), only known binary and ternary pnictides were observed. $Sr_2Cu_6P_5$

Table 2. Refined Atomic Parameters for $Sr_2Cu_6P_5$ and $Eu_2Cu_6P_5$

Compound	$Sr_2Cu_6P_5$			$Eu_2Cu_6P_5$		
Atom, site	*z*	Occ	B_{eq}, Å^2[a]	*z*	Occ	B_{eq}, Å^2
A (00*z*)	0.3512(1)	1	1	0.3516(1)	1	0.5(1)
Cu1 (1/20*z*)	0.0522(1)	1	1	0.0517(2)	1	0.5(1)
Cu 2 (1/201/4)	1/4	1	1	1/4	1	1.0(1)
P1 (001/2)	1/2	1	1	1/2	1	0.3(1)
P2 (00*z*)	0.1049(2)	1	1	0.1059(4)	1	0.3(1)
P3 (00*z*)	0.1981(1)	1	1	0.1980(4)	1	0.3(1)

[a]Not refined in the experiment.

dx.doi.org/10.1021/ic301033h | Inorg. Chem. 2012, 51, 8948−8955

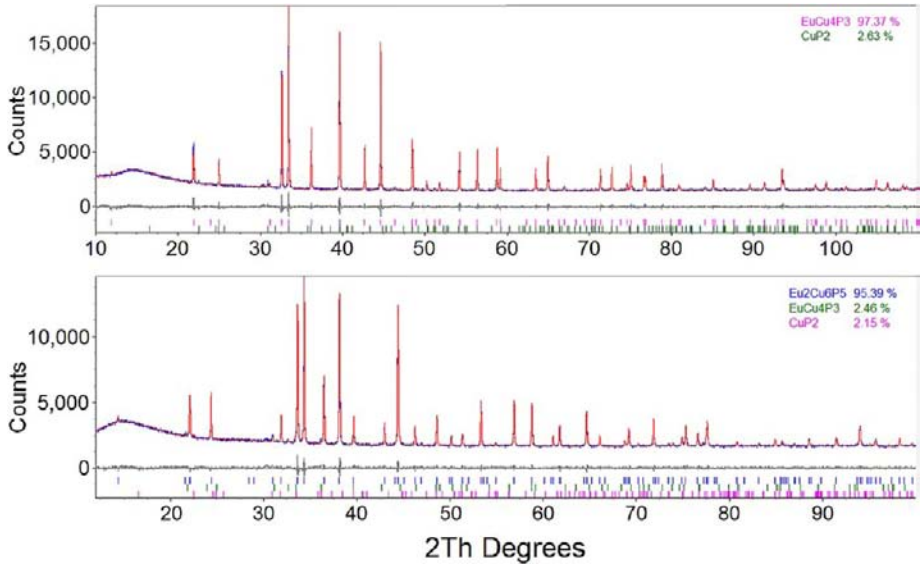

Figure 2. Final Rietveld refinement plots for $EuCu_4P_3$ (top) and $Eu_2Cu_6P_5$ (bottom).

and $Eu_2Cu_6P_5$ are analogs of $Ca_2Cu_6P_5$ while $EuCu_4P_3$ remains as yet the only copper−pnictide representative of the $BaMg_4Si_3$ structure type. The increase of the unit cell volume in the $Ca_2Cu_6P_5$−$Eu_2Cu_6P_5$−$Sr_2Cu_6P_5$ series is consistent with the ionic radii of Ca^{2+}, Eu^{2+}, and Sr^{2+}.[17] It is worth noting that bond distances in $EuCu_{2-x}P_2$[8] and $EuCu_4P_3$ are very close to those in the intergrowth $Eu_2Cu_6P_5$ structure (Table 2).

The crystal structure was confirmed by the TEM analysis. The SAED patterns of $EuCu_4P_3$ taken along [001] and [100] zone axes are shown in Figure 3(a). These patterns can be consistently indexed on a primitive tetragonal lattice with cell parameters $a \approx 4.1$ Å and $c \approx 7.4$ Å. No reflection conditions were observed, which suggests *P*4/*mmm* as the most symmetric space group. The SAED patterns of $Eu_2Cu_6P_5$ are represented in Figure 3(b). They can be indexed on a body-centered tetragonal lattice with the cell parameters $a \approx 4.1$ Å and $c \approx 24.6$ Å. The only reflection condition is *hkl*: $h + k + l = 2n$, which is consistent with the space group *I*4/*mmm*.

A real space investigation on the crystal structure of $EuCu_4P_3$ and $Eu_2Cu_6P_5$ has been performed using the HAADF-STEM technique. The corresponding images are shown in Figure 4. The intensity of the bright dots in such images is related to the average atomic number (Z) of the projected atomic column and roughly scales as $I \sim Z^n$ (where n is between 1 and 2). Therefore, the brighter dots correspond to Eu and weaker dots correspond to Cu, whereas the P columns are not revealed due to their relatively low Z number. The "143" structure ($EuCu_4P_3$) can be represented by the following sequence of the atomic layers: −Eu−P−Cu_2−P′−Cu_2−P−Eu-P−Cu_2−P′−Cu_2−P− (where P′ denotes the phosphorus atomic layer sandwiched between two Cu_2 layers). The "265" structure ($Eu_2Cu_6P_5$) is obtained by an ordered alternation of "122" and "143" slabs. The "122" structure ($EuCu_2P_2$) is composed of the following sequence of atomic layers along the c axis: −Eu−P−Cu_2−P−Eu-P-Cu_2−P− and does not contain a P′ layer. On the HAADF-STEM images the layers of P′ atoms appear darker, which allows us to distinguish the "122" and "143" slabs unambiguously. The insets in Figure 4 are the calculated HAADF-STEM images using the atomic parameters of the structures (Tables 2 and 3). These calculated images are clearly in good agreement with the experimental ones.

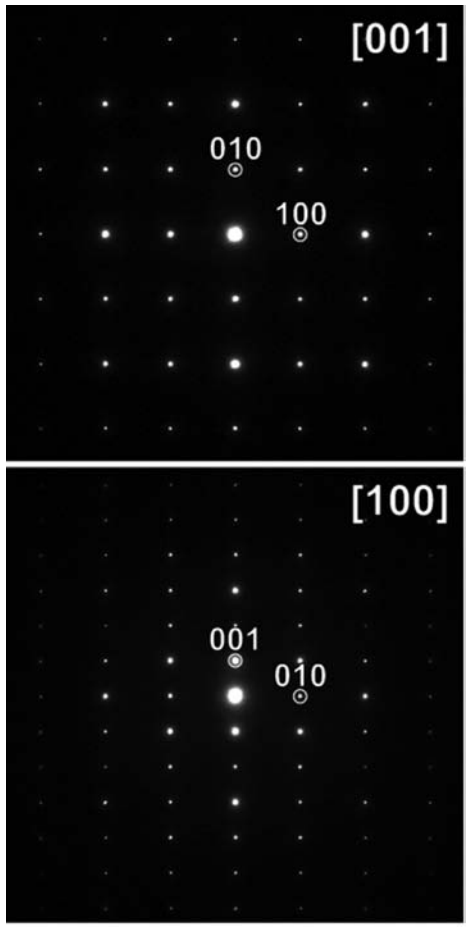

Figure 3. Electron diffraction patterns along the [001] and [100] axes for $EuCu_4P_3$.

Planar defects were observed in the $Eu_2Cu_6P_5$ sample. They are visible in the HAADF-STEM images (Figure 5). The "265" (i.e., "122" + "143") matrix can form coherent intergrowth with slabs of "143" and "387" (2 × "122" + "143") structures (upper image). They can be distinguished according to the number of the Eu layers in the constituent "122" and "143" building

dx.doi.org/10.1021/ic301033h | *Inorg. Chem.* 2012, 51, 8948−8955

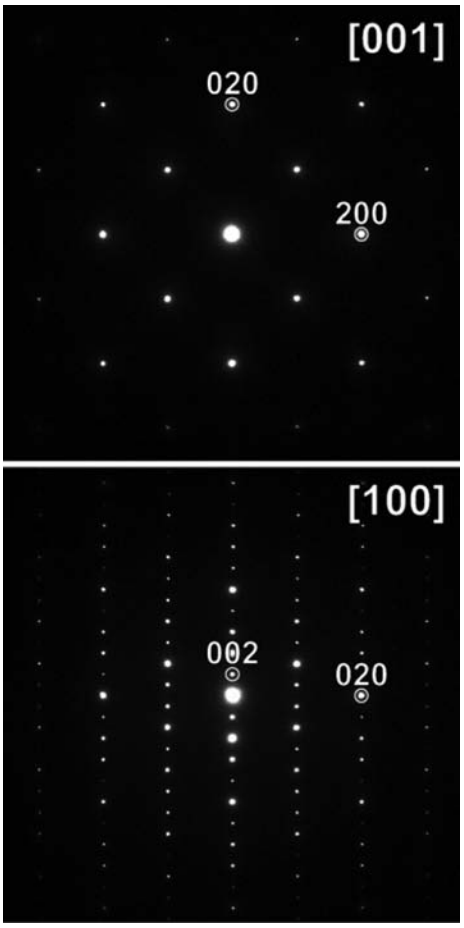

Figure 4. Electron diffraction patterns along the [001] and [100] axes for $Eu_2Cu_6P_5$.

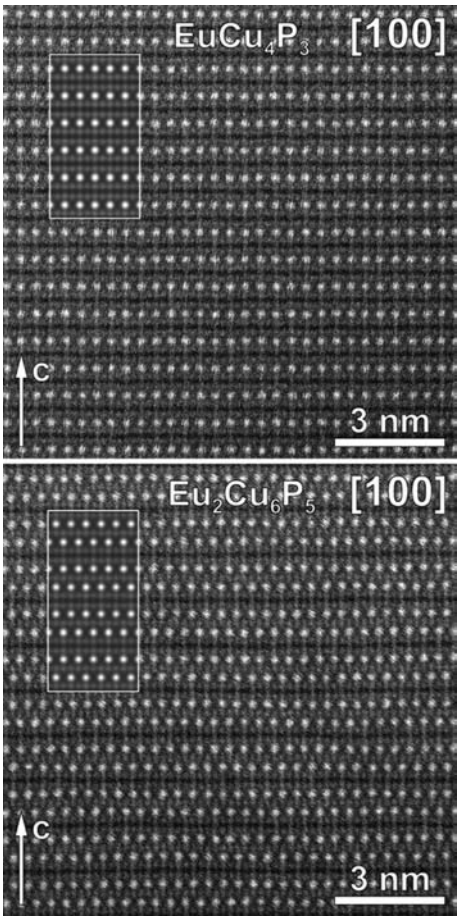

Figure 5. HAADF-STEM images of $EuCu_4P_3$ and $Eu_2Cu_6P_5$ taken along the [100] zone axis. Insets show the simulated STEM images, which were calculated using the structure parameters from Table 1 for the thickness of 48 Å. The size of the insets is $6b \times 6c$ for $EuCu_4P_3$ and $6b \times 2c$ for $Eu_2Cu_6P_5$.

blocks. The lamellas of "143" and "387" are marked with 1 and 3, correspondingly, and the slabs of the matrix "265" structure are marked as 2.

Lamellae of the "143" and "387" phases can grow through the entire crystal (Figure 5, top) or terminate inside the crystal by forming defects in the stacking of the atomic layers (Figure 5, bottom). These defects can be isolated or arrange themselves into a more complex cluster of defects composed of the array of the equi-spaced steps. Either an individual defect or ordered arrays change the sequence of the building units of the structure. It can be directly seen on the HAADF-STEM image (Figure 5, bottom) that an individual defect changes the stacking of "143"−"265" on the left side of the defect to "265″-"143" on the right side and the cluster of defects changes the sequence of "265" × 6-"143" (left) to "143"−"265" × 6 (right). Therefore, both these defects are caused by the introduction of a single "143" lamella. The array of steps is marked by white lines on the HAADF-STEM image; they have an orientation close to the (110) plane of the "122"structure. One can notice that this plane can be flipped along the *b*-axis, changing the orientation to the $(1\bar{1}0)$ plane, whereas the spacing between two adjacent defects remains the same. Apparently, a shift of the steps requires only a short-range diffusion, which allows the rearrangement of the defects into an equi-spaced array, thereby minimizing the free energy associated with the defects. A similar kind of defects has been observed in hexagonal perovskites.[16]

Transport and Magnetic Properties. Transport measurements on $Sr_2Cu_6P_5$ (not shown) reveal metallic behavior from room temperature down to 2 K, the lowest temperature of our experiment, with no indication for superconductivity or any other kind of phase transition. We find a shallow minimum in $\rho(T)$ around 12 K followed by an increase of about 3% on cooling to 2 K. The temperature dependence of the resistivity in zero magnetic field for $Eu_2Cu_6P_5$ and $EuCu_4P_3$ for 2 K $\leq T \leq$ 290 K is shown in Figures 6 and 7. Both materials show metallic behavior over the entire temperature range without any indication for superconductivity. However, the data reveal various anomalies, indicative of phase transitions, which manifest themselves in abrupt changes in the temperature dependence of $\rho(T)$. For $Eu_2Cu_6P_5$, we find a sharp drop in the resistivity below 34 K as typically observed below a transition to long-range magnetic order.[18] As will be described below in more detail, this feature is ascribed to a ferromagnetic transition of the local 4*f* Eu moments. The transition temperature of T_C = (34 ± 0.03) K can be determined more precisely from the position of the pronounced maximum in $d\rho/dT$, shown in the inset of Figure 6, in accordance with general arguments on critical scattering.[18] The $\rho(T)$ curve of $EuCu_4P_3$, depicted in the main panel of Figure 8, exhibits at least two kink-like anomalies, one at T_1 = 70 K and the other at T_2 = 40 K, clearly visible in the $d\rho/dT$ data in the inset. These results indicate that

dx.doi.org/10.1021/ic301033h | *Inorg. Chem.* 2012, 51, 8948−8955

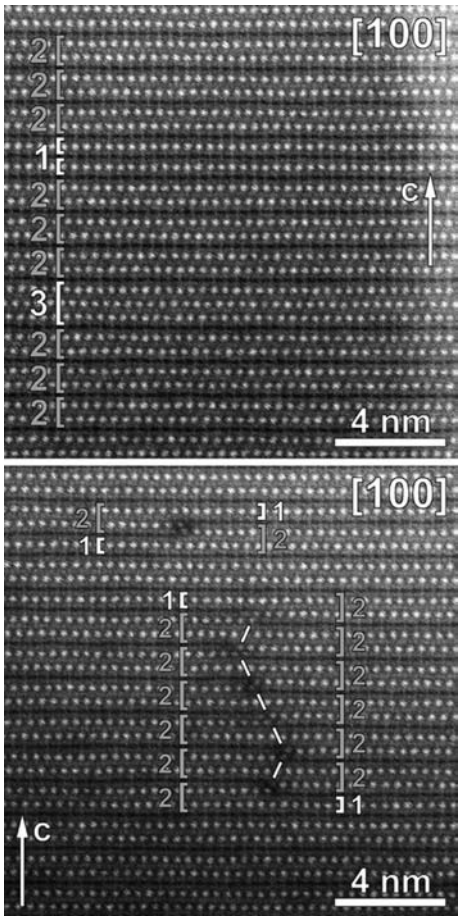

Figure 6. HAADF-STEM image of $Eu_2Cu_6P_5$, demonstrating planar defects .The upper image shows the coherent intergrowth of the "265" structure with the lamellas of "143" and "387" structures. The lower image illustrates how the insertion of the "143" evokes the interleaving building blocks inside the crystal. The distinctive lamellas are marked with brackets and indicated by the number of Eu sublayers (1, 2, and 3) in the "143", "265", and "387" lamellas, respectively.

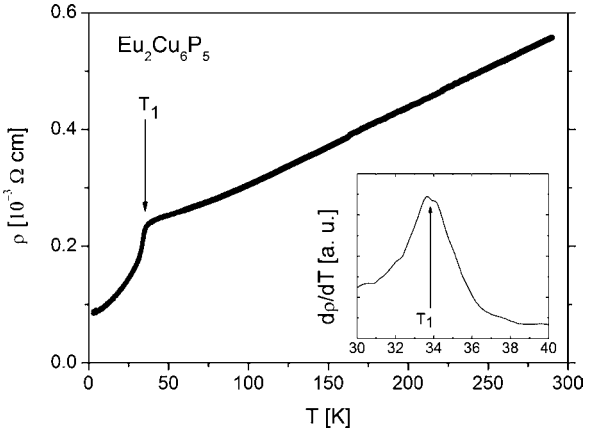

Figure 7. Temperature dependence of the resistivity of $Eu_2Cu_6P_5$ over the whole temperature range. The arrow at T_1 indicates the position of the pronounced maximum in $d\rho/dT$ shown in the inset.

in $EuCu_4P_3$ there are at least two phase transitions in the temperature range under investigation. Given that no magnetic impurities were found in the sample (Figure 2), we believe that the multiple transitions are an intrinsic property of $EuCu_4P_3$.

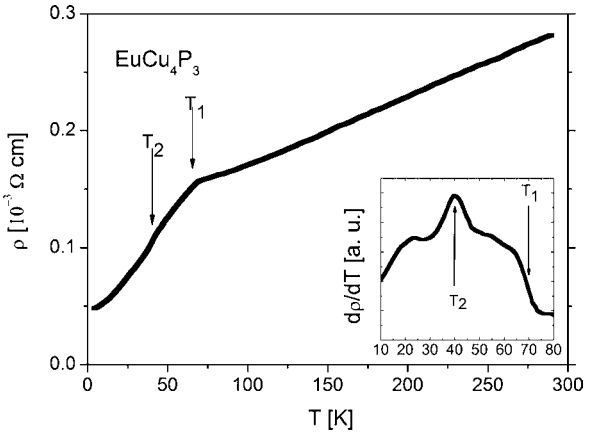

Figure 8. Temperature dependence of the resistivity of $EuCu_4P_3$ over the whole temperature range. The inset shows $d\rho/dT$ in the temperature range 10−80 K. Arrows labeled T_1 and T_2 correspond to the positions of the two most clearly pronounced anomalies in $d\rho/dT$.

The main panel of Figure 9 shows the molar magnetic susceptibility, $\chi_{mol}(T)$, of $EuCu_4P_3$ and $Eu_2Cu_6P_5$ as a function

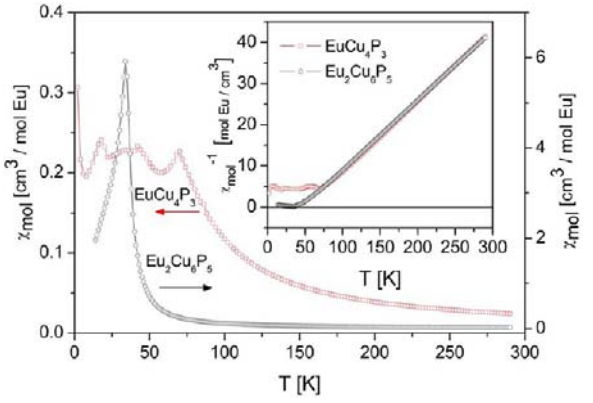

Figure 9. Temperature dependence of the magnetic susceptibility per mole Eu, $\chi(T)$, of $EuCu_4P_3$ (left scale) and $Eu_2Cu_6P_5$ (right scale). Inset shows the same data plotted as $\chi(T)^{-1}$ vs T.

of temperature. Both materials are characterized by large values of χ_{mol} and a paramagnetic high-temperatures regime, i.e., an increase of χ_{mol} upon cooling, typical for Eu-derived 4*f* local-moment magnetism. The sharp peaks in χ_{mol} following at lower temperatures mark the phase transitions into long-range magnetic order of those 4*f* moments. In order to determine the sign and the magnitude of the predominant magnetic interactions in the materials, the inverse susceptibility is plotted in the inset of Figure 9. For both compounds $\chi_{mol}^{-1}(T)$ follows an in-T linear, i.e., Curie−Weiss-type, behavior down to about 150 K. From fits to the experimental data for 150 K $\leq T \leq$ 290 K, Weiss temperatures of $\theta_W = 45 \pm 0.3$ K for $Eu_2Cu_6P_5$ and 52 $\pm$ 0.3 K for $EuCu_4P_3$ are derived. These numbers indicate that the magnetic interactions between the local 4*f* Eu moments in these compounds have predominantly a ferromagnetic character.

To obtain information about the valence state of the Eu ions for the two compounds, we plot in Figure 10 the temperature dependence of the effective magnetic moment (in CGS units) $n_{eff} = (N_A \cdot \mu_B^2/3k_B)^{1/2} \times (T \cdot \chi_{mol})^{1/2}$ per Eu ion, where N_A is Avogadro's number, μ_B the Bohr magneton, and k_B the

dx.doi.org/10.1021/ic301033h | Inorg. Chem. 2012, 51, 8948−8955

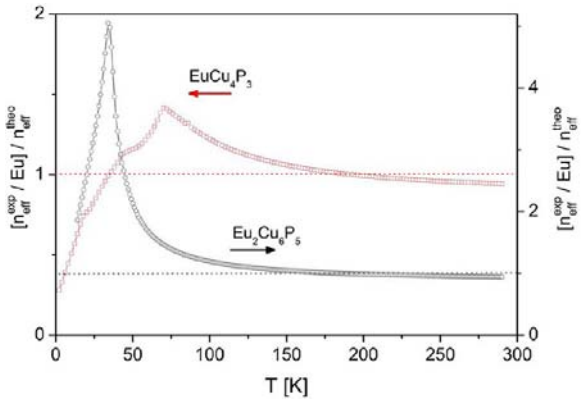

Figure 10. Temperature variation of the effective magnetic moment, $n_{eff}(T)$, of $EuCu_4P_3$ (left scale) and $Eu_2Cu_6P_5$ (right scale) per Eu^{2+} ion normalized to the free-ion value of Eu^{2+}.

Boltzmann constant. The data of n_{eff} were normalized to the theoretical value of the free Eu^{2+} ion of 7.94 μ_B. Note that for Eu^{3+}, $n_{eff} = 0$ according to the Hund's rules, but due to the small crystal-field splitting of the ground-state multiplet, the population of excited magnetic states is finite below room temperature.[19] This typically leads to experimental n_{eff} values of about 3.5 μ_B at 300 K for Eu^{3+}-containing materials.[19] Figure 9 shows $n_{eff}(T)$ of $EuCu_4P_3$ (left scale) and $Eu_2Cu_6P_5$ (right scale). From 290 K down to the sharp maximum in $n_{eff}(T)$, corresponding to the phase transition temperature T_1, there is a continuous increase in n_{eff}, again reflecting the mean ferromagnetic character of the correlations in the paramagnetic state of both compounds. One important result that follows from Figure 10 is that for both compounds the n_{eff} values in the temperature range above about 200 K are close to the value of the free Eu^{2+} ion, clearly indicating that for both materials the Eu valence state is predominantly 2+. The temperature dependence of n_{eff} is much stronger for $Eu_2Cu_6P_5$ as compared to $EuCu_4P_3$. The sharp maximum of n_{eff} for both compounds clearly marks the transition into a low-temperature magnetically ordered state. For $EuCu_4P_3$, one finds an ordering temperature of 69.9 K, a value which coincides with the position of the kink in the $\rho(T)$ data at T_1. The two other anomalies at 42.5 and 18.3 K, seen as shoulders in the $n_{eff}(T)$ data, indicate further phase transitions, in accordance with the structures observed in the $\rho(T)$ data, and more clearly in $d\rho/dT$ in the inset of Figure 9. For $Eu_2Cu_6P_5$, a single sharp maximum in $n_{eff}(T)$ is located at 34.6 K, again consistent with the position of the maximum in the $d\rho/dT$ data.

To explore the character of the magnetic transitions for both compounds in more detail, magnetization measurements were performed at low temperature, i.e., within the ordered state. Figure 11 shows the results of the isothermal magnetization of $Eu_2Cu_6P_5$ taken at $T = 2$ K. The low-field magnetization curve is shown in the main panel on expanded scales. The data reveal a small but distinct hysteretic behavior, characteristic of a soft ferromagnet. The inset of Figure 10 displays the magnetization over an extended field range up to the saturation. The saturated moment of approximately 6.4 μ_B per Eu ion is consistent with the observations made for other Eu^{2+}-containing systems[20] (as, e.g., 6.8 μ_B at $T \rightarrow 0$ for EuO[21]). The ferromagnetic nature of the transition at $T_C = 34$ K in this compound is also corroborated by temperature-dependent measurements in various fields (not shown). In the data taken at 0.4 mT, for example, the smallest field of our experiments, we observed a strong increase in χ_{mol}

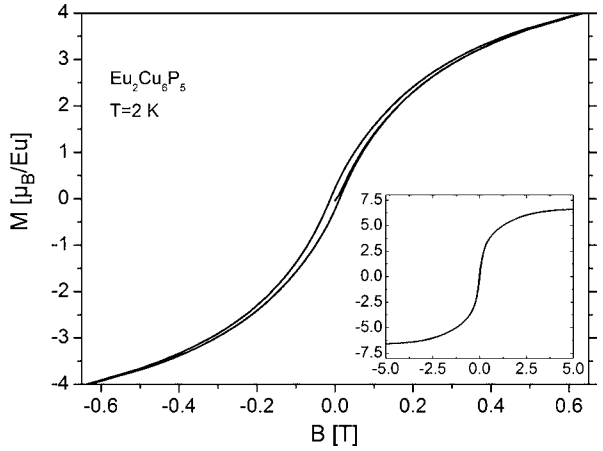

Figure 11. Isothermal magnetization of $Eu_2Cu_6P_5$ taken at $T = 2$ K. Main panel: Hysteresis together with the virgin curve at small fields. Inset: The same magnetization curve over the whole field range investigated, i.e., up to the saturation.

upon cooling. At around 34 K, the increase in χ_{mol} is strongest, and a hysteresis opens upon further cooling. Both observations are clear indications for a ferromagnetic transition.

Compared to $Eu_2Cu_6P_5$, shown in Figure 12, the low-temperature magnetic behavior of $EuCu_4P_3$, shown in Figure

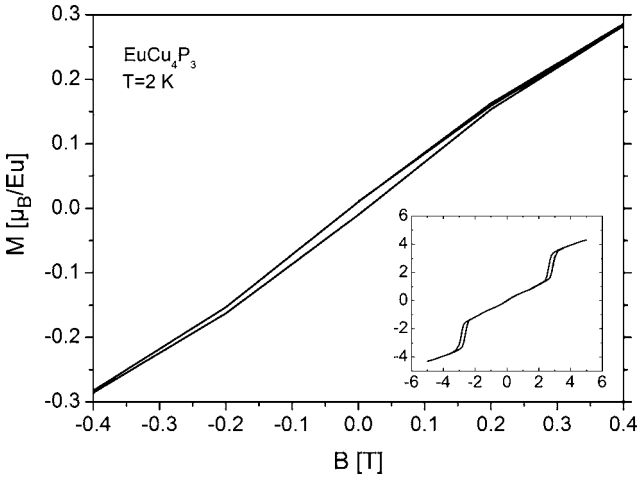

Figure 12. Isothermal magnetization of $EuCu_4P_3$ taken at $T = 2$ K. Main panel: Blow-up of low-field data. Inset: Magnetization curve over the whole field range investigated.

12, is more complex. The full magnetization curve for the fields -5 T $\leq B \leq 5$ T is shown in the inset of Figure 11. On the scale of the magnetization used in the inset, the data lack clear indications for hysteretic behavior at fields $|B| < 2$ T. For larger fields $|B| \approx 2.5$ T, however, the magnetization yields step-like changes accompanied by a distinct hysteresis upon increasing and decreasing the field. Moreover, a careful inspection of the low-field data in the main panel of the figure uncovers a very small hysteresis also in the low-field range, i.e., -0.4 T $\leq B \leq$ 0.4 T. We stress that on increasing the field to $|B| = 5$ T, the saturation is not yet reached. Although the interactions are predominantly ferromagnetic, the present data do not allow for a full elucidation of the character of the magnetic state in this compound.

dx.doi.org/10.1021/ic301033h | Inorg. Chem. 2012, 51, 8948−8955

DISCUSSION

Crystal Chemistry and Relationship to Other Layered *Anti*-Fluorites. The crystal structures of $EuCu_{2-x}P_2$, $Eu_2Cu_6P_5$, and $EuCu_4P_3$ are represented in Figure 1. A common feature of the three structures (as well as $A_2Cu_6P_5$ and $AeCu_{2-x}P_2$ with A = Ca and Sr) is the formation of interlayer P−P dumbbells, which suggests an alternative description of these structures as 3D frameworks formed by 2D arrays of Cu−P and P−P bonds with the latter hosting the A^{2+} cations (A = Ca, Sr, and Eu). This differs the structures of $ACu_{2-x}P_2$, $EuCu_4P_3$, and $A_2Cu_6P_5$ from those of related copper chalcogenides like $BaCu_2S_2$,[22] KCu_4S_3,[23a] or $Tl_2Cu_7S_4Sb$,[24] where there are no interlayer bonds between the chalcogens, and the structures are truly two-dimensional.

Another peculiar feature of the "265" and "143" structures is the presence of the "inner" phosphorus atom (designated as P′) linked only to copper atoms. Because the P−P distances in the dumbbells assume a single bond,[25] these P atoms may be assigned with an oxidation state of −2 (P_2^{4-} dumbbells). The Cu−P distances in our compounds (2.41−2.44 Å) are typical to those observed in other layered Cu^I phosphides (2.39−2.42 Å).[6c,d,7a] Assuming the oxidation states of Cu and A to be +1 and +2, respectively, we see that at least in the "265" structure, the P′ atoms also have an oxidation state −2 and appear to be one electron-deficient. Delocalization of this electron deficiency over the $[Cu_6P_5]$ and $[Cu_4P_3]$ frameworks (which may be suggested from relatively small differences in the length of Cu−P and Cu−P′ bonds) is a likely reason for the metallic behavior of the Eu compounds. This behavior appears to be particularly similar to that of the 2D metal KCu_4S_3 where the double tetrahedral $[Cu_4S_3]$ layers also appear to be one electron-deficient.[23a] The comparison of the composition and crystal structure of the new $A_2Cu_6P_5$ and $EuCu_4P_3$ compounds with those of the previously known members of layered copper−chalcogenide and copper−pnictide *anti*-fluorites reveals a clear and nontrivial tendency: the double tetrahedral layers, $[Cu_4E_3]$ (E = chalcogen or pnicogen) are electron-deficient in all structures where they are observed. In the structures of ACu_4Ch_3 (A = Tl, K, Rb, Cs, or NH_4; Ch = S or Se),[23] the isolated Cu_4E_3 layers (not linked via interlayer dumbbells) bonds are also one-electron deficient. This electron deficiency seems to be a necessary condition for their existence. For instance, the $BaCu_4S_3$ compound, formally corresponding to the "electron-precise" version of KCu_4S_3, adopts a completely different structure.[26] The same applies also to the triple $[Cu_6S_4]^-$ slab in $TlCu_6S_4$: an electron-precise compound $TlCu_7S_4$ adopts another structure.[27] In addition, in the mixed-layer compound $Tl_2Cu_7SbS_4$,[24] both the $[Cu_2S_2]^-$ and $[Cu_5SbS_2]^-$ slabs are one electron-deficient, assuming Tl is univalent. This peculiarity is observed only for the Cu-bearing compounds: isostructural ternary pnictides of alkaline metals and zinc or cadmium are electron-precise.[28] Similarly, the oxidation states can be easily assigned in $BaMg_4Tt_3$ as $Ba^{2+}(Mg^{2+})_4Tt^{4+}(Tt_2)^{6-}$.[10]

Despite the overall structural similarities, the compounds of alkaline earth (Ca, Sr) and rare-earth (Eu) metals demonstrate some differences. The oxidation state of +2 for both Ca and Sr can be compared with the valence state of Eu in $EuCu_4P_3$, which may be slightly above +2. As yet, we have no direct evidence for this except the experimentally determined n_{eff} falling below the theoretically expected value for Eu^{2+} by about 7% at room temperature, pointing toward a formal valence of Eu to be slightly higher than 2+. This corresponds to the presence of 10−15% Eu^{3+} moments, carrying 3.5 μ_B at 300 K. The hypothesis permits us to explain the uniqueness of $EuCu_4P_3$ among the pnictides: the "143" structure is not formed with alkaline earth cations (which can be only divalent), and $EuCu_4As_3$ is not stable because even low concentrations of Eu^{3+} may be redox-incompatible with As^{3-} (or As^{2-} in As_2^{4-}dumbbells). Our preliminary attempts to stabilize the $CaCu_4P_3$ structure by injecting the "lacking" electrons via changing the composition into $Ca_{1-x}Gd_xCu_4P_3$ showed no success.

Transport and Magnetic Properties. The magnetic properties of $Eu_2Cu_6P_5$ and $EuCu_4P_3$ are governed by the partially filled inner 4*f* shell of the Eu ions. In general, the electronic configuration of the *f* shell in Eu-containing compounds is either $4f^6$ or $4f^7$, corresponding to a Eu valence state of 3+ or 2+, respectively. Because both configurations are energetically close to each other, valence fluctuations may result giving rise to a noninteger mean valence of the Eu ions as, e.g., observed in the intermediate-valence systems $EuCu_2Si_2$[29] and $EuNi_2P_2$.[30] For the present compounds, however, the Eu valence is rather close to 2+, i.e., a $4f^7$ configuration, with some indications for a noninteger-valence state of 2.1−2.15+ for $EuCu_4P_3$.

Both Eu-containing compounds clearly demonstrate a ferromagnetic ordering, with a rather complex and yet unveiled nature of transitions for $EuCu_4P_3$. It should be noted that prior to this work, there was only one report on magnetic properties of a compound containing Eu, Cu, and P.[31] However, $Eu_xBa_{8-x}Cu_{16}P_{30}$ adopts a completely different crystal structure and orders antiferromagnetically at about 3 K.

CONCLUSIONS

We have discovered three new representatives of layered copper pnictides, including one of the "143" type yet not observed in this family. While $Sr_2Cu_6P_5$ exhibits simple metallic conductivity, both Eu-containing compounds are metals and order ferromagnetically. Whereas $Eu_2Cu_6P_5$ features a $4f^7$ (Eu^{2+}) ground state, $EuCu_4P_3$ shows signals for a possible presence of Eu in a slightly higher oxidation state of about +2.10 to 2.15.

The magnetic system for both compounds interacts with the conduction electrons as evidenced by the reduction in the resistivity upon cooling in the magnetically ordered state as a consequence of the freezing out of spin-disorder scattering. As far as superconductivity is concerned, none of the materials reveal any indication for a superconducting transition. Given the presence of long-range order of stable 4*f*-derived local Eu moments with strong ferromagnetic interactions, and the significant coupling of these moments to the conduction electrons in $Eu_2Cu_6P_5$ and $EuCu_4P_3$, the absence of superconductivity here is not surprising. Therefore, $LiCu_2P_2$[3a] remains the only superconducting copper pnictide, and even in this case, superconductivity appears to be very sensitive to some subtle and not fully understood experimental details, as the first result was not reproduced in some of the later work.[3b]

ASSOCIATED CONTENT

Supporting Information

Crystallographic data for $Sr_2Cu_6P_5$, $Eu_2Cu_6P_5$, and $EuCu_4P_3$. This material is available free of charge via the Internet at http://pubs.acs.org.

dx.doi.org/10.1021/ic301033h | *Inorg. Chem.* 2012, 51, 8948−8955

AUTHOR INFORMATION

Corresponding Author

*E-mail: charkin@inorg.chem.msu.ru.

Notes

The authors declare no competing financial interest.

ACKNOWLEDGMENTS

The authors thank Prof. Dr. P. E. Kazin (Chemistry Department of Moscow State University) for valuable discussions. The support of the Russian Foundation for Basic Research (Grant No. 10-03-00681-a), Moscow State University Development Program, and the German Science Foundation via the priority program SPP 1458 is acknowledged. Part of this work has been performed in the framework of the ERC project "Countatoms".

REFERENCES

(1) Kamihara, Y.; Watanabe, T.; Hirano, M.; Hosono, H. *J. Am. Chem. Soc.* **2008**, *130*, 3296.

(2) (a) Clarke, S. J.; Adamson, P.; Herkelrath, S. J. C.; Rutt, O. J.; Parker, D. R.; Pitcher, M. J.; Smura, C. F. *Inorg. Chem.* **2008**, *47*, 8473. (b) Jöhrendt, D.; Hosono., H.; Hoffmann, R.-D.; Pöttgen, R. *Z. Kristallogr.* **2011**, *226*, 435.

(3) (a) Han, Jiantao; Zhou, Jianshi; Cheng, Jinguang; Goodenough, J. B. *J. Am. Chem. Soc.* **2010**, *132*, 908. (b) Han, F.; Zhu, X.; Mu, G.; Zeng, B.; Cheng, P.; Shen, B.; Wen, H. H. *J. Am. Chem. Soc.* **2011**, *133*, 1751.

(4) (a) Xu, G.; Ming, W.; Yao, Y.; Dai, X.; Zhang, S.-C.; Fang, Z. *Europhys. Lett.* **2008**, *82*, 67002. (b) Singh, D. J.; Du, M.-H. *Phys. Rev. Lett.* **2008**, *100*, 237003.

(5) (a) Jemetio Feudjio, J. P.; Doert, T.; Rademacher, O.; Boettcher, P. *J. Alloys Compd.* **2002**, *338*, 93. (b) Yang, X. X.; Lu, Y.-M.; Zhou, S. K.; Mao, S. Y.; Mi, J. X.; Man, Z. Y.; Zhao, J.- T. *Mater. Sci. Forum* **2005**, *475*, 861. (c) Mozharivsky, Yu.; Kaczorowski, D.; Franzen, H. F. *J. Solid State Chem.* **2000**, *155*, 259.

(6) (a) Kaczorowski, D.; Potel, M.; Noël, H. *J. Solid State Chem.* **1994**, *112*, 228. (b) Albering, J. H.; Jeitschko, W. *Z. Naturforsch. B* **1996**, *51*, 257. (c) Wells, D. M.; Ringe, E.; Kaczorowski, D.; Gnida, D.; André, G.; Haire, R. G.; Ellis, D. E.; Jbers, J. A. *Inorg. Chem.* **2011**, *50*, 576. (d) Abe, H.; Yoshii, K. *J. Solid State Chem.* **2002**, *165*, 372.

(7) (a) Cava, R. J.; Zandbergen, H. W.; Krajewski, J. J.; Siegrist, T.; Hwang, H. Y.; Batlogg, B. *J. Solid State Chem.* **1997**, *129*, 250. (b) Kaiser, J. W.; Jeitschko, W. *Z. Naturforsch. B* **2002**, *57*, 165.

(8) Mewis, A. *Z. Naturforsch. B* **1980**, *35*, 141.

(9) Dünner, J.; Mewis, A.; Röpke, M.; Michels, G. *Z. Anorg. Allgem. Chem.* **1995**, *621*, 1523.

(10) Pilchowski, I.; Mewis, A. *Z. Anorg. Allg. Chem.* **1990**, *581*, 173.

(11) Kaczorowski, D.; Noël, H.; Troć, R. *J. Less-Comm. Met.* **1991**, *170*, 255.

(12) Zürcher, F.; Wengert, S.; Nesper, R. *Inorg. Chem.* **1999**, *38*, 4567.

(13) TOPAS V3: General Profile and Structure Analysis Software for Powder Diffraction Data, User's Manual; Bruker AXS: Karlsruhe, Germany, 2003.

(14) Koch,C. Ph.D. Thesis, Arizona State University, Phoenix, AZ, 2002.

(15) *Handbook of Chemistry and Physics*; Weast, R.C., Eds.; CRC: Cleveland, OH, 1969; pp E129−E134.

(16) (a) Van Tendeloo, G.; Amelinckx, S.; Darriet, B.; Bontchev, R.; Darriet, J.; Weill, F. *J. Solid State Chem.* **1994**, *108*, 314. (b) Abakumov, A. M.; Shpanchenko, R. V.; Antipov, E. V.; Lebedev, O.I .; Van Tendeloo, G.; Amelinckx, S. *J. Solid State Chem.* **1998**, *141*, 492.

(17) Shannon, R. D. *Acta Cryst. A* **1976**, *32*, 751.

(18) Fisher, M. E.; Langer, J. S. *Phys. Rev. Lett.* **1968**, *20*, 665.

(19) Lueken, H.; *Magnetochemie*, B. G. Teubner, Stuttgart, Leibzig, 1999.

(20) (a) Grandjean, F.; Gerard, A.; Braun, D. J.; Jeitschko, W. *J. Phys. Chem. Solids* **1984**, *45*, 877. (b) Felner, I. *J. Phys. Chem. Solids* **1975**, *36*, 1063.

(21) Taylor, K. N. R.; Darby, M. I. *Physics of Rare Earth Solids*; Chapman and Hall, LTD.: London, 1972.

(22) Saeki, M.; Onoda, M.; Nozaki, H. *Mater. Res. Bull.* **1988**, *23*, 603.

(23) (a) Brown, D. B.; Zubieta, J.; Vella, P. A.; Wrobleski, J. T.; Watt, T.; Hatfield, W. E.; Day, P. *Inorg. Chem.* **1980**, *19*, 1945. (b) Klepp., K.; Boller, H.; Völlenkle, H. *Monatsh. Chem.* **1980**, *111*, 727. (c) Purdy, A. *Chem. Mater.* **1998**, *10*, 692.

(24) Makovicky, E.; Johan, Z.; Karup-Møller, S. *Neu. Jahrb. Miner. Abh.* **1980**, *138*, 122.

(25) (a) Von Schnering, H. G. *Angew. Chem.* **1981**, *93*, 44. (b) Von Schnering, H. G.; Hönle, W. *Chem. Rev.* **1988**, *88*, 243.

(26) Iglesias, J. E.; Pachali, K. E.; Steinfink, H. *Mater. Res. Bull.* **1972**, *7*, 1247.

(27) (a) Berger, R.; Eriksson, L. *J.Less-Com. Met.* **1990**, *161*, 165. (b) Norén, L.; Larsson, K.; Delaplane, R. G.; Berger, R. *J. Alloys Compd.* **2001**, *314*, 114.

(28) (a) Türck, R.; Carrillo-Cabrera, W.; Peters, K.; Hönle, W.; Von Schnering, H. G. *Z. Kristallogr. Suppl.* **1992**, *5*, 250. (b) He, H.; Tyson, C.; Bobev, S. *Inorg. Chem.* **2011**, *50*, 8375.

(29) Bauminger, R.; Froindlich, D.; Nowik, I.; Ofer, S.; Felner, I.; Mayer, I. *Phys. Rev. Lett.* **1973**, *30*, 1053.

(30) Nagarajan, R.; Sampathkumaran, E. V.; Gupta, L. C.; Vijayaraghavan, R.; Prabhawalkar, V.; Bhaktdarshan, Padalia, B. D. *Phys. Lett. A* **1981**, *84*, 275.

(31) Kovnir, K.; Stockert, U.; Budnyk, S.; Prots, Yu.; Baitinger, M.; Paschen, S.; Shevelkov, A. V.; Grin, Yu. *Inorg. Chem.* **2011**, *50*, 10387.